Orbital Fluctuations in the Different Phases of $LaVO_3$ and YVO_3

M. De Raychaudhury,[1,2] E. Pavarini,[3,4] and O. K. Andersen[1]

[1]*Max-Planck-Institut für Festkörperforschung, Heisenbergstrasse 1, D-70569 Stuttgart, Germany*
[2]*S. N. Bose National Centre for Basic Sciences, Kolkata 700098, India*
[3]*Institut für Festkörperforschung, Forschungzentrum Jülich, D-52425 Jülich, Germany*
[4]*CNISM-Dipartimento di Fisica "A. Volta", Università di Pavia, Via Bassi 6, I-27100 Pavia, Italy*
(Received 13 February 2007; published 17 September 2007)

We investigate the importance of quantum orbital fluctuations in the orthorhombic and monoclinic phases of the Mott insulators $LaVO_3$ and YVO_3. First, we construct *ab initio* material-specific t_{2g} Hubbard models. Then, by using dynamical mean-field theory, we calculate the spectral matrix as a function of temperature. Our Hubbard bands and Mott gaps are in very good agreement with spectroscopy. We show that in orthorhombic $LaVO_3$, quantum orbital fluctuations are strong and that they are suppressed *only* in the monoclinic 140 K phase. In YVO_3 the suppression happens already at 300 K. We show that Jahn-Teller *and* $GdFeO_3$-type distortions are both crucial in determining the type of orbital and magnetic order in the low temperature phases.

The Mott insulating t_{2g}^2 perovskites $LaVO_3$ and YVO_3 exhibit an unusual series of structural and magnetic phase transitions (Fig. 1) with temperature-induced magnetization-reversal phenomena [1] and other exotic properties [2,3]. While it is now recognized that the V-t_{2g} orbital degrees of freedom and the strong Coulomb repulsion are the key ingredients, it is still controversial whether classical (orbital order) [1,4–8] or quantum (orbital fluctuations) [2,9] effects are responsible for the rich physics of these vanadates.

At 300 K, $LaVO_3$ and YVO_3 are orthorhombic paramagnetic Mott insulators. Their structure (Fig. 2) can be derived from the cubic perovskite ABO_3, with $A = $ La, Y and $B = $ V, by tilting the VO_6 octahedra in alternating directions around the **b** axis and rotating them around the **c** axis. This $GdFeO_3$-type distortion is driven by AO covalency which pulls a given O atom closer to one of its four nearest A neighbors [10,11]. Since the Y 4d level is closer to the O 2p level than the La 5d level, the AO covalency increases when going from $LaVO_3$ to YVO_3 and, hence, the shortest AO distance decreases from being 14% to being 20% shorter than the average, while the angle of tilt increases from 12° to 18°, and that of rotation from 7° to 13° [12,13]. Finally, the A cube is deformed such that one or two of the ABA body diagonals are smaller than the average by, respectively, 4% and 10% in $LaVO_3$ and YVO_3. These 300 K structures are determined mainly by the strong covalent interactions between O 2p and the empty $B e_g$ and $A d$ orbitals, hardly by the weak interactions involving $B t_{2g}$ orbitals, and they are thus very similar to the structures of the t_{2g}^1 La and Y titanates [10,11].

The t_{2g}^2 vanadates, however, have a much richer phase diagram than the t_{2g}^1 titanates. At, respectively, 140 K and 200 K, $LaVO_3$ and YVO_3 transform to a monoclinic structure in which **c** is turned slightly around **a** whereby the two subcells along **c**, related by a horizontal mirror

plane in the orthorhombic structure, become independent (Fig. 2). Most important: a sizable (3%–4%) Jahn-Teller (JT) elongation of a VO bond, that along **y** in cells 1 and 4, and along **x** in cells 3 and 2, deforms the VO_6 octahedra. At about 140 in $LaVO_3$ and 116 K in YVO_3, antiferro*magnetic* (AFM) C-type order develops (ferromagnetic stacking of antiferromagnetic ab layers). At 77 K, YVO_3 recovers the orthorhombic structure and the magnetic order changes from C to G type (3D-AFM), while the long VO bond becomes that along **x** in cells 1 and 3, and along **y** in 2 and 4.
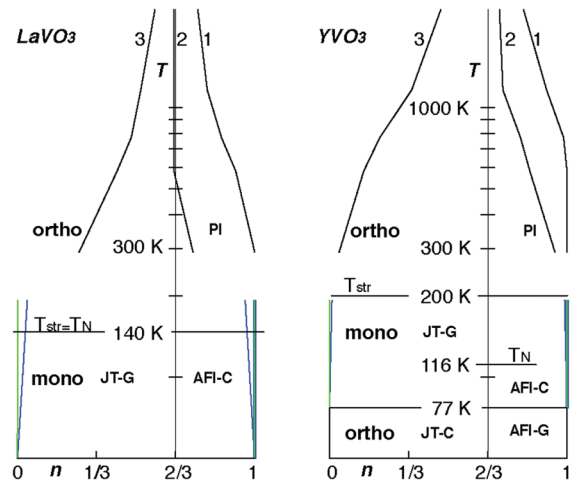

FIG. 1 (color). Temperature-dependent structural and magnetic phases of $LaVO_3$ and YVO_3. The lines show LDA + DMFT (quantum Monte Carlo [21]) results for the occupations, n, of the three t_{2g} crystal-field orbitals, 1, 2, and 3 (Table I). Black lines: orthorhombic phases. Green and blue lines: monoclinic, sites 1 and 3 (see Fig. 2). For each structure we calculated the occupations down the temperature at which the orbital polarizations are essentially complete ($T \sim 200$ K) and then extrapolated in a standard way [21] to $T = 0$ K.
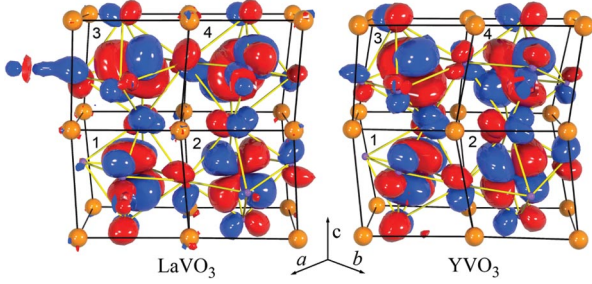
FIG. 2 (color). Primitive cell containing four ABO_3 units. A ions are orange; B ions are at the centers of yellow O octahedra. In terms of the primitive translation vectors, **a**, **b**, and **c** the global **x**, **y**, and **z** axes, directed approximately along the BO bonds, are $\mathbf{x} = \mathbf{a}/(2 + 2\alpha) + \mathbf{b}/(2 + 2\beta)$, $\mathbf{y} = -\mathbf{a}/(2 + 2\alpha) + \mathbf{b}/(2 + 2\beta)$, and $\mathbf{z} = (\mathbf{c} - \mathbf{c} \cdot \mathbf{b})/(2 + 2\gamma)$. Here, α, β, and γ are small and $|\mathbf{x}| = |\mathbf{y}| = |\mathbf{z}| = 3.92$ Å (3.82 Å) for $LaVO_3$ (YVO_3). The B-containing bc-plane glide mirrors [with translation $(\mathbf{b} - \mathbf{a})/2$] unit 1 in 2 and 3 in 4, and exchanges the local, B-centered x and y coordinates. In the orthorhombic $Pbnm$ structure (but not in the monoclinic $P2_1/a$ structure), the A-containing ab plane mirrors unit 1 in 3 and 2 in 4. The empty crystal-field orbitals $|3\rangle_i$ of the monoclinic phase were put on sites $i = 1, 2, 3, 4$. Red (blue) indicate positive (negative) lobes.

It has been suggested [1] that these phase transitions are driven by the changes in a static orbital order (OO) following the observed pattern of JT distortions [4,14]. According to this JT-OO model, which assumes that the crystal field (CF) is due to the oxygen octahedra, the t_{2g} orbital which is *most* antibonding with the O $2p$ orbitals, i.e., $|sz\rangle$, where s is the direction of the *short* in-plane VO bond, is *empty*; the other two t_{2g} orbitals, due to Hund's rule coupling, are *singly* occupied. This OO is C type in the orthorhombic structure and G type in the monoclinic structure. Later, this JT-OO model was challenged by a theory which assumes that the two highest orbitals, $|xz\rangle$ and $|yz\rangle$, are basically degenerate so that orbital *fluctuations* play a key role [2,9]. Recently, *ab initio* LDA + U [6] calculations gave support to the JT-OO model.

In this Letter we show that in $LaVO_3$ quantum effects are strong down to 300 K; however, they become negligible in the C-type AFM monoclinic phase. For YVO_3 orbital fluctuations are suppressed already at 300 K, and the 77 K magnetic transition is associated with a change of OO. We show that the CF splittings result not only from the JT-, but also from the $GdFeO_3$-type distortions, and thus OO is intermediate between C and G type. The influence of the JT- and the $GdFeO_3$-type distortion is, respectively, stronger and weaker than in the t_{2g}^1 titanates [10,11,15].

The electronic structure is calculated with the LDA + DMFT (local density approximation + dynamical mean-field theory) method [16], fully accounting for the orbital degrees of freedom [11]. First, we compute the LDA bands with the Nth-order muffin-tin-orbital (NMTO) method [17]; we obtain (for all structures) $\frac{1}{3}$-filled t_{2g} bands separated by a ~0.5 eV gap from the empty e_g bands and by a

~2 eV gap from the filled O $2p$ bands. Next, we Löwdin downfold to Vt_{2g} and remove the energy dependence of the downfolded orbitals by "N-ization" [17]. These orbitals are strongly localized, having Vt_{2g} character only in their heads. Symmetric orthonormalization finally yields localized [18] t_{2g} Wannier functions and their corresponding Hamiltonian, H^{LDA}. The many-body Hamiltonian is then a material-specific t_{2g} Hubbard model, $\hat{H} = \hat{H}^{LDA} + \hat{U}$, where for the on-site Coulomb repulsion, $\hat{U}$, we use the conventional expression [19], $\hat{U} = \frac{1}{2}\sum_{im\sigma,m'\sigma'} U_{m\sigma,m'\sigma'} \times n_{im\sigma} n_{im'\sigma'}$, where $n_{im\sigma} = c^\dagger_{im\sigma} c_{im\sigma}$, and $c^\dagger_{im\sigma}$ creates an electron with spin σ in a t_{2g} Wannier orbital m at site i. The screened on-site Coulomb interaction is $U_{m\sigma,m'\sigma'} = U\delta_{m,m'}\delta_{\sigma,-\sigma'} + (U' - J\delta_{\sigma,\sigma'})(1 - \delta_{m,m'})$, where J is the exchange term and $U' = U - 2J$ the average Coulomb repulsion. We solve $\hat{H}$ in DMFT [20], using a quantum Monte Carlo [21] impurity solver and working with the full self-energy matrix, $\Sigma_{mm'}(\omega)$ [11]. Note that inversion is the only point symmetry of the V sites. The spectral matrix on the real ω axis is obtained by analytic continuation [22]. We use $U = 5$ eV and $J = 0.68$ eV, values close to theoretical [14] and experimental [23] estimates, which also give the correct mass renormalizations or Mott gaps for orthorhombic t_{2g}^1 V/Ti oxides using the same computational scheme [10,11].

Let us start by describing the LDA t_{2g} bands in the orthorhombic 300 K phase. Remarkably, the CF orbitals $|j\rangle_i$ (Table I, $j = 1, 2, 3$), obtained by diagonalizing the on-site i block of H^{LDA}, the hopping integrals $t^{i,i'}_{j,j'}$ (Table II), the t_{2g} band shapes and bandwidth W (Fig. 3) are rather similar to those of the t_{2g}^1 titanates. These similarities [24] are due to the similarity of the crystal structures. Like in the titanates, the CFs are essentially determined by the $GdFeO_3$-type distortion, mainly via the A-ligand field, specifically the AB and AOB covalency. However, in the vanadates the CF splittings are about half those of the respective titanates and the CF orbitals [25] and the hopping integrals are less deformed by cation covalency [24]. This is due to the Ti $\rightarrow$ V substitution [26]: since V is on the right of Ti in the periodic table, the V $3d$ level is closer to the O $2p$ and further from the A d level than the Ti $3d$. Thus the sensitivity of the B t_{2g} Wannier functions to $GdFeO_3$-type distortions decreases, while the sensitivity to JT increases.

Now, turning on the Coulomb repulsion transforms the metallic LDA density of states (DOS) into the spectral matrix of a Mott insulator (Fig. 3). For $LaVO_3$, the Mott gap is ~1 eV, in accord with optical conductivity data [27], and the Hubbard bands are centered around -1.5 eV and 2.5 eV, in very good agreement with photoemission and inverse photoemission experiments [28]. For YVO_3, the gap is slightly larger, ~1.2 eV, in accord with optical data [27], and the Hubbard bands are centered around -1.5 eV and 3 eV, in agreement with photoemission experiments [28].

TABLE I. LDA crystal-field (CF) levels with respect to the t_{2g}^1 Fermi level, $\epsilon_j/$meV ($j = 1, 2, 3$), LDA CF orbitals at site i, $|j\rangle_i$, in terms of the cubic orbitals, $|xy\rangle$, $|xz\rangle$, and $|yz\rangle$ in the global **x**, **y**, **z** axes defined in Fig. 2. n_j are LDA occupations. Orbitals at equivalent sites (see Fig. 2): $|j\rangle_2$ ($|j\rangle_4$) is $|j\rangle_1$ ($|j\rangle_3$) with $x \leftrightarrow y$; for the *Pbnm* structures $|j\rangle_3$ is $|j\rangle_1$ with $z \rightarrow -z$.

$|j\rangle_i$	ϵ_j	$|xy\rangle$	$|xz\rangle$	$|yz\rangle$	n_j	ϵ_j	$|xy\rangle$	$|xz\rangle$	$|yz\rangle$	n_j
	Pbnm LaVO$_3$ (300 K)					*Pbnm* YVO$_3$ (300 K)				
$|1\rangle_1$	419	0.44	0.24	0.86	0.78	303	0.56	−0.21	0.80	0.96
$|2\rangle_1$	472	0.34	0.84	−0.42	0.63	383	0.83	0.17	−0.54	0.53
$|3\rangle_1$	511	−0.83	0.48	0.29	0.59	510	−0.02	0.96	0.27	0.51
	*P*2$_1$/*a* LaVO$_3$ (10 K)					*P*2$_1$/*a* YVO$_3$ (100 K)				
$|1\rangle_1$	393	0.46	0.11	0.88	0.82	285	0.78	−0.30	0.55	0.97
$|2\rangle_1$	471	0.86	0.16	−0.48	0.63	360	0.49	−0.25	−0.83	0.58
$|3\rangle_1$	539	−0.19	0.98	−0.03	0.55	525	0.39	0.92	−0.05	0.55
$|1\rangle_3$	441	0.71	−0.46	−0.53	0.76	345	0.77	0.20	−0.60	0.88
$|2\rangle_3$	453	0.08	0.77	−0.64	0.66	405	0.62	−0.44	0.65	0.56
$|3\rangle_3$	531	−0.70	−0.41	−0.58	0.57	547	−0.13	−0.88	−0.46	0.45
						Pbnm YVO$_3$ (65 K)				
$|1\rangle_1$						313	0.64	−0.26	0.72	0.98
$|2\rangle_1$						394	0.72	0.53	−0.45	0.60
$|3\rangle_1$						517	−0.27	0.81	0.53	0.42

The Mott gaps in the vanadates are somewhat *larger* than in the titanates, for which the measured gaps are ~ 0.2 eV in LaTiO$_3$ and ~ 1 eV in YTiO$_3$ [27], in line with LDA + DMFT results [11]. This could appear surprising: orbital degeneracy increases the critical ratio for the Mott transition, U_c/W, by enhancing the effective bandwidth, and the enhancement is stronger the closer the system is to half filling [29]. So the gap should be smaller for a t_{2g}^2 than for a t_{2g}^1 system; everything else remaining the same. However, the Hund's rule exchange energy, J, strongly suppresses this enhancement, as shown for half filling in Ref. [30]. For $n = \frac{1}{6}$ and $n = \frac{1}{3}$, and using a threefold degenerate Hubbard model with a rectangular DOS, $T = 770$ K, and $J/W \sim \frac{1}{3}$ (like in the vanadates where $J/W = 0.68/1.9$), we find that the metal to insulator transition occurs for $U'/W \sim 1.5$ when $n = \frac{1}{6}$, and for $U'/W \sim 1.3$ when $n = \frac{1}{3}$. So the Hund's-rule coupling dominates, and thus the vandates can have larger gaps than the titanates.

Like for the titanates [11], diagonalization of the DMFT occupation matrix yields three eigenvectors nearly identical to the LDA CF orbitals. For LaVO$_3$ at 770 K, the Coulomb repulsion only slightly increases the orbital polarization by changing the occupations as follows: $0.78 \rightarrow 0.87$, $0.63 \rightarrow 0.65$, and $0.59 \rightarrow 0.48$. Thus, surprisingly, orbital fluctuations are sizable and remain so down to room temperature: $n_3 = 0.26$ at 290 K. Because of the stronger cation covalency in YVO$_3$, the Coulomb repulsion causes substantial orbital polarization already at 770 K (see Fig. 1). At 300 K, we find that only $c_{2\sigma}^{\dagger} c_{1\sigma}^{\dagger} |0\rangle$, paramagnetic with $S = 1$, is occupied. Thus, YVO$_3$ is orbitally ordered well above the magnetic phase transition; since, at site 1, $|3\rangle_1 \approx |xz\rangle$ (see Table I) is empty and thus $|xy\rangle$ and $|yz\rangle$ are $\approx$ singly occupied, the OO happens to agree with the prediction of the JT-OO model [4,6,14] ($|3\rangle_1 \approx -|3\rangle_3 \approx |xz\rangle$, $|3\rangle_2 \approx -|3\rangle_4 \approx |yz\rangle$), even though the CF is caused mainly by the GdFeO$_3$-type distortion.

What happens in the JT-distorted low temperature phases? The rms values of the hopping integrals hardly change, so W remains ~ 1.9 eV, but individual hopping integrals do change, even in the $|xy\rangle$, $|xz\rangle$, $|yz\rangle$ representation. Most affected are the CF orbitals (see Table I).

For LaVO$_3$, the CF splittings increase; this, in addition to the low temperature, lets the Coulomb repulsion suppress quantum effects entirely. At sites 1 and 2, the occupied state is in accord with the JT distortion (at site 1 $|xy\rangle$ and $|yz\rangle$ are singly occupied and $|3\rangle_1 \approx |xz\rangle$ is empty; at site 2, by symmetry, the empty state is $|3\rangle_2 \approx |yz\rangle$; see Fig. 2 and Table I) but this is not the case at sites 3 and 4 ($|3\rangle_3 \neq -|yz\rangle$, $|3\rangle_4 \neq -|xz\rangle$). A static mean-field calculation (pseudopotential-based LDA + U) [6] yields empty states not far from ours [31], but, without analyzing the results, the OO was ascribed to the JT distortions. In contrast, we find that the CF orbitals depend crucially also on the GdFeO$_3$-type distortions and that the OO is not of G-type, but is intermediate between C and G type.

For YVO$_3$, the CF splittings are similar to those of the 300 K phase, but quantum effects are negligible (Fig. 1). On *all* sites in the monoclinic structure the *empty* orbital is almost the same as in the orthorhombic 300 K phase so OO does *not* follow the JT distortions ($|3\rangle_1 \approx -|3\rangle_3 \approx |xz\rangle$, $|3\rangle_2 \approx -|3\rangle_4 \approx |yz\rangle$), but is almost C type. In the orthorhombic 77 K phase, the empty orbital at site 1, $|3\rangle_1$, only roughly equals $|xz\rangle$. Our results are consistent with resonant x-ray scattering [5] and magnetization [1] data. LDA + U [6] yields results close to ours [31].

TABLE II. Hopping integrals $t_{j,j'}^{i,i'}/$meV from site i to a site $i' = i + l\mathbf{x} + m\mathbf{y} + n\mathbf{z}$, in the basis ($j, j'$) of crystal-field orbitals. Here $i = 1$ and ($P2_1/a$ only) $i = 3$ (see Fig. 1). Notice that $t_{j,j'}^{i,i+\mathbf{z}} = t_{j',j}^{i+\mathbf{z},i}$ and $t_{j,j'}^{i,i+\mathbf{x}} = t_{j',j}^{i,i+\mathbf{y}}$. For *Pbnm* structures only: $t_{j,j'}^{i,i+\mathbf{z}} = t_{j',j}^{i,i+\mathbf{z}}$.

|	La *Pbnm*			La *P*2$_1$/*a*, site 1			La *P*2$_1$/*a*, site 3			Y *Pbnm*			Y *P*2$_1$/*a*, site 1			Y *P*2$_1$/*a*, site 3			Y *Pbnm* (65 K)		
j, j'\lmn	001	100	010	001	100	010	001	100	010	001	100	010	001	100	010	001	100	010	001	100	010
1, 1	130	−65	−65	85	−39	−39	85	−159	−159	−13	−17	−17	−49	−84	−84	−49	−92	−92	−35	−34	−34
1, 2	9	−37	−198	27	−110	−127	−36	−65	98	−63	−102	−157	−20	−117	−62	−46	−73	−169	−38	−66	−195
1, 3	119	104	−7	154	31	−155	153	90	23	46	66	−138	30	11	−170	26	80	−91	52	100	−68
2, 2	193	47	47	−133	−84	−84	−133	94	94	86	−48	−48	72	−6	−6	72	25	25	142	−28	−28
2, 3	26	13	9	−57	76	73	−140	110	30	38	5	20	−112	9	94	118	−41	30	67	−27	7
3, 3	36	−152	−152	65	−38	−38	65	−109	−109	202	−66	−66	183	−48	−48	183	−63	−63	173	−61	−61
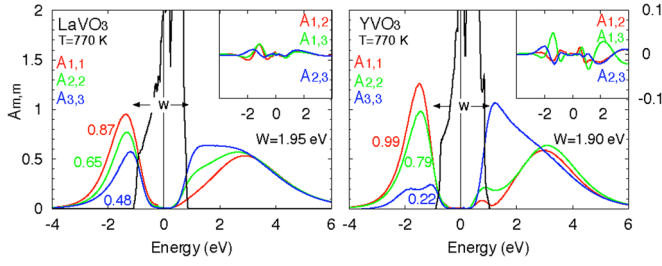
FIG. 3 (color online). LDA + DMFT spectral matrix $A_{m,m'}$ in the crystal-field basis. The off-diagonal terms are ~5 times smaller than in LDA. In black, the LDA DOS.

Finally, we find that the monoclinic structure favors C-type magnetic order over G type by increasing some hopping integrals $t_{j,j'}^{i,i'}$ (Table II) to the empty orbital $|3\rangle$ along the **c** direction. Assuming complete OO, conventional theory yields, for the superexchange couplings,

$$J_{\mathrm{SE}}^{i,i'} \sim \frac{1 + J/U}{U + 2J} \sum_{j,j' \leq 2} |t_{j,j'}^{i,i'}|^2 - \frac{J/U}{U - 3J} \sum_{j \leq 2} (|t_{j,3}^{i,i'}|^2 + |t_{3,j}^{i,i'}|^2)$$

with j, j' CF orbitals and i, i' neighboring sites. We find that C-type order ($J_{\mathrm{SE}}^{i,i+\mathbf{z}} < 0$, $J_{\mathrm{SE}}^{i,i+\mathbf{x}} = J_{\mathrm{SE}}^{i,i+\mathbf{y}} > 0$) is favored over G type, for which all couplings are positive, if $J/U \gtrsim 0.16$. While the actual values of $J_{\mathrm{SE}}^{i,i'}$ are sensitive to details [6,7,10], this provides a microscopic explanation of C-type order in monoclinic LaVO$_3$ and YVO$_3$, the change from C to G type across the structural phase transition in YVO$_3$, and thus could also explain the magnetization-reversal phenomena [1].

In conclusion, we find that the orthorhombic LaVO$_3$ is one of the few Mott insulators which exhibits large quantum effects at room temperature. This is not the case for YVO$_3$ (and t_{2g}^1 titanates [11]). In the low temperature phases, orbital fluctuations are negligible for both vanadates. This supports the view [1,4,14] that the magnetic structures of the vanadates can be explained by orbital order. Recent LDA + U [6] and LDA + PIRG (path-integral renormalization group) [8] calculations agree with this, but previous literature ascribed OO mainly to JT distortions. In contrast, we proved that both the JT *and* the GdFeO$_3$-type distortions are crucial for the CF orbitals and their hopping integrals and thus for the type of orbital and magnetic order. The effects of the GdFeO$_3$-type distortions are weaker and those of JT stronger than in t_{2g}^1 titanates; their interplay is responsible for the rich phase diagram of the vanadates.

We thank E. Koch, A. I. Lichtenstein, S. Biermann, and A. Georges for discussions and J. Nuss for graphics support. Computations were done on the Jülich BlueGene. M. D. thanks the MPG Partnergroup program.

[1] Y. Ren *et al.*, Nature (London) **396**, 441 (1998); Phys. Rev. B **67**, 014107 (2003).

[2] C. Ulrich *et al.*, Phys. Rev. Lett. **91**, 257202 (2003).

[3] J.-Q. Yan, J.-S. Zhou, and J. B. Goodenough, Phys. Rev. Lett. **93**, 235901 (2004).

[4] H. Sawada *et al.*, Phys. Rev. B **53**, 12 742 (1996); H. Sawada and K. Terakura, *ibid.* **58**, 6831 (1998); T. Mizokawa, D. I. Khomskii, and G. A. Sawatzky, *ibid.* **60**, 7309 (1999).

[5] M. Noguchi *et al.*, Phys. Rev. B **62**, R9271 (2000); M. Takahashi and J. I. Igarashi, *ibid.* **65**, 205114 (2002).

[6] Z. Fang and N. Nagaosa, Phys. Rev. Lett. **93**, 176404 (2004). With their parameters ($U_{\mathrm{eff}} = 3$ eV, $J/U \sim 0.2$), we find (in meV) for $P2_1/a$ YVO$_3$ (LaVO$_3$): $J_{\mathrm{SE}}^{i,i+\mathbf{z}} = -1.8\,(-4.1)$, $J_{\mathrm{SE}}^{1,1+\mathbf{x}} = 0.06\,(3.0)$, and $J_{\mathrm{SE}}^{3,3+\mathbf{x}} = 7.1\,(7.6)$.

[7] I. V. Solovyev, Phys. Rev. B **74**, 054412 (2006).

[8] Y. Otsuka and M. Imada, J. Phys. Soc. Jpn. **75**, 124707 (2006).

[9] G. Khaliullin, P. Horsch, and A. M. Oles, Phys. Rev. Lett. **86**, 3879 (2001); G. Khaliullin, Prog. Theor. Phys. Suppl. **160**, 155 (2005).

[10] E. Pavarini, A. Yamasaki, J. Nuss, and O. K. Andersen, New J. Phys. **7**, 188 (2005).

[11] E. Pavarini *et al.*, Phys. Rev. Lett. **92**, 176403 (2004).

[12] P. Bordet *et al.*, J. Solid State Chem. **106**, 253 (1993).

[13] G. R. Blake *et al.*, Phys. Rev. B **65**, 174112 (2002).

[14] T. Mizokawa and A. Fujimori, Phys. Rev. B **54**, 5368 (1996).

[15] M. Mochizuki and M. Imada, Phys. Rev. Lett. **91**, 167203 (2003); New J. Phys. **6**, 154 (2004).

[16] V. Anisimov *et al.*, J. Phys. Condens. Matter **9**, 7359 (1997); A. I. Lichtenstein and M. I. Katsnelson, Phys. Rev. B **57**, 6884 (1998).

[17] O. K. Andersen and T. Saha-Dasgupta, Phys. Rev. B **62**, R16219 (2000); Bull. Mater. Sci. **26**, 19 (2003); Ref. [10].

[18] F. Lechermann *et al.*, Phys. Rev. B **74**, 125120 (2006).

[19] R. Fresard and G. Kotliar, Phys. Rev. B **56**, 12 909 (1997).

[20] A. Georges, G. Kotliar, W. Kraut, and M. J. Rozenberg, Rev. Mod. Phys. **68**, 13 (1996).

[21] J. E. Hirsch and R. M. Fye, Phys. Rev. Lett. **56**, 2521 (1986).

[22] J. E. Gubernatis, M. Jarrell, R. N. Silver, and D. S. Sivia, Phys. Rev. B **44**, 6011 (1991).

[23] S. Miyasaka, Y. Okimoto, M. Iwama, and Y. Tokura, Phys. Rev. B **68**, 100406(R) (2003).

[24] See Eqs. (19)–(20), (23)–(26), and Fig. 18 of Ref. [10].

[25] Compare orbitals in Fig. 2 with Fig. 14 of Ref. [10].

[26] To prove this we performed LDA calculations using the titanates crystal structure and replacing Ti with V.

[27] T. Arima, Y. Tokura, and J. B. Torrance, Phys. Rev. B **48**, 17 006 (1993); Y. Okimoto *et al.*, *ibid.* **51**, 9581 (1995); S. Miyasaka, Y. Okimoto, and Y. Tokura, J. Phys. Soc. Jpn. **71**, 2086 (2002); A. A. Tsvetkov *et al.*, Phys. Rev. B **69**, 075110 (2004).

[28] H. F. Pen *et al.*, Phys. Rev. B **59**, 7422 (1999); K. Maiti and D. D. Sarma, *ibid.* **61**, 2525 (2000).

[29] O. Gunnarsson, E. Koch, and R. M. Martin, Phys. Rev. B **54**, R11026 (1996); E. Koch, O. Gunnarsson, and R. M. Martin, *ibid.* **60**, 15 714 (1999).

[30] J. E. Han, M. Jarrell, and D. L. Cox, Phys. Rev. B **58**, R4199 (1998).

[31] In Ref. [6] occupations are not for Wannier functions ($n_{t_{2g}} < 2$), so a full comparison is not possible.